SAND2015-10864C

Evaluation of PV Frequency-Watt Function for Fast Frequency Reserves

J. Neely, *Member IEEE*, J. Johnson, *Member IEEE*, J. Delhotal, S. Gonzalez, M. Lave, *Member IEEE*,
Sandia National Laboratories
Albuquerque, NM, USA
jneely@sandia.gov

***Abstract*—Increasing the penetration of distributed renewable sources, including photovoltaic (PV) sources, poses technical challenges for grid management. The grid has been optimized over decades to rely upon large centralized power plants with well-established feedback controls, but now non-dispatchable, renewable sources are displacing these controllable generators. By programming autonomous functionality into distributed energy resources—in particular, PV inverters—the aggregated PV resources can act collectively to mitigate grid disturbances. This paper focuses on the problem of frequency regulation. Specifically, the use of existing IEC 61850-90-7 grid support functions to improve grid frequency response using a frequency-watt function was investigated. The proposed approach dampens frequency disturbances associated with variable irradiance conditions as well as contingency events without incorporating expensive energy storage systems or supplemental generation, but it does require some curtailment of power to enable headroom for control action. Thus, this study includes a determination of the trade-offs between reduced energy delivery and dynamic performance. This paper includes simulation results for an island grid and hardware results for a testbed that includes a load, a 225 kW diesel generator, and a 24 kW inverter.**

Keywords—photovoltaics, IEC advanced functions, advanced inverters, frequency regulation, frequency-watt, PV curtailment

I. Introduction

With plans to replace conventional power generation with renewable power, utilities fear large frequency and voltage excursions resulting from variability of renewable power generation, reduced mechanical inertia (for power electronic-coupled systems), and reduced grid support, i.e. voltage and frequency regulation. Some island power systems have realized high renewable penetration in a short time frame, and technical issues encountered therein are regarded by many as predictive for larger power systems in the U.S. In these island grids, PV systems are often required to also install expensive smoothing batteries [1] to mitigate the effect of PV fluctuations on the grid. The requirements are driven by concerns that the variability of renewable generators will overpower frequency regulating reserves provided by traditional generators, resulting in large frequency swings. These strict, expensive requirements could be lightened if the entire system were stabilized (rather than smoothing each plant individually). One method involves the implementation of grid support functions in grid-connected photovoltaic sources [2]. In this paper, the proposed method is studied for the power grid on the island of Lanai.

A. Lanai Power System

Lanai is a 140.5 square mile Hawaiian island with approximately 3,200 residents in 1,150 households, living mostly in Lanai city. Fig. 1 presents an overview of the power system which includes a 10.4 MW diesel power plant, three 12.47 kV distribution circuits, the 1.2 MW La Ola PV power plant [3], and a 6 MW peak load.

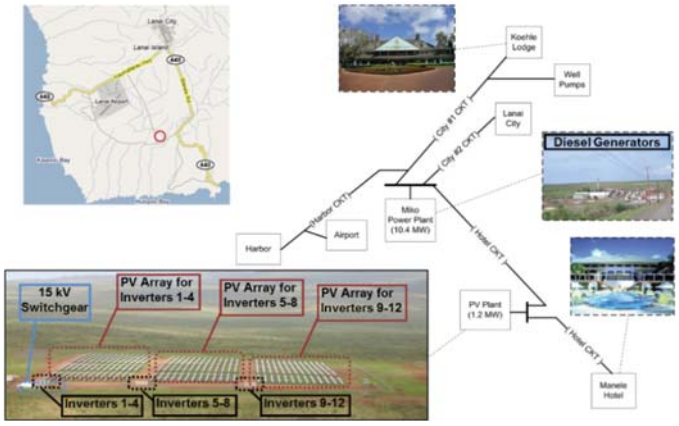

Fig. 1. Overview of the Lanai power system; reproduced from [1]

A previous study of the 1.2 MW PV plant in Lanai, HI demonstrated that real power curtailment alone was an effective tool to reduce PV ramp rates and assist with frequency stability [3]. Unfortunately, when performing this control strategy, much of the DC power is 'left on the array.' In this work, the Lanai power system is modeled and simulated assuming PV resources are configured to implement frequency-watt control. Evaluations of techno-economic performance are determined over a full day using a simplified model implemented in MATLAB [4]; and fault performance is evaluated over short time frames using a high-fidelity model developed in General Electric's *Positive Sequence Load Flow* (GE's PSLF). Several scenarios are considered with different PV penetrations and grid-support function settings. In addition, a testbed was assembled using select hardware at the *Distributed Energy Technology Laboratory* (DETL), including a diesel generator and a PV inverter with frequency-watt capability. This testbed was used to evaluate the frequency-watt function's ability to mitigate frequency deviations on a small power system with large steps in load.

This work was supported by the U.S. Department of Energy SunShot program under Award Number 29092. Sandia National Laboratories is a multi-program laboratory managed and operated by Sandia Corporation, a wholly owned subsidiary of Lockheed Martin Corporation, for the U.S. Department of Energy's National Nuclear Security Administration under contract DE-AC04-94AL85000.

B. Frequency-Watt Control

Figure 2 shows an example of the *International Electrotechnical Commission* (IEC) *Technical Report* (TR) 61850-90-7 [5] FW22 frequency-watt curve with a deadband which curtails the output power at nominal grid frequency, allows generation to increase at grid frequencies below F_2 (if the power is available), and decreases generation when the grid frequency rises above F_3.

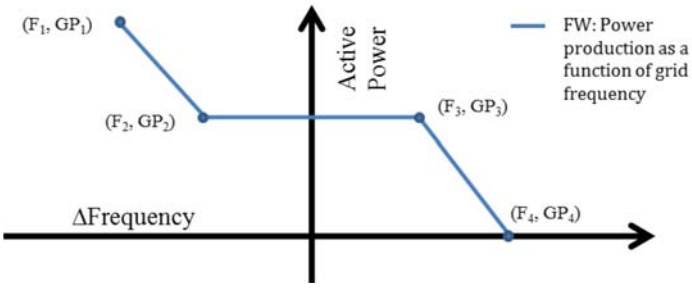

Fig. 2. Frequency-Watt control curve [5]

The next section provides details of the simulation models developed for this study in MATLAB and PSLF. Section III presents simulation results that evaluate the trade-offs of energy loss and frequency deviation. In particular, use of frequency-watt control is compared to that of fixed curtailment, and it is shown to provide a superior trade-off in frequency response versus energy loss. Section IV presents the results of hardware experiments intended to demonstrate and evaluate the application of frequency-watt to a power system that mimics an island grid. Finally, Section V provides conclusions and cites future work.

II. Simulation Models for the Lanai Power System

The Lanai power system was evaluated in simulation using irradiance data collected at the 1.2 MW La Ola PV power plant located there. Specifically, irradiance data was used in concert with the Sandia-developed Wavelet Variability Model [6]-[9] to compute available PV power. Four irradiance profiles ranging from low to high variability were identified for the study. To evaluate the power system dynamics, a simplified MATLAB model was developed to efficiently simulate the day-long effects of PV variability and frequency-watt function parameters on frequency response and renewable energy production. In addition, a model was developed using PSLF to evaluate grid response using high-fidelity component models of the island grid. Both models were developed for three PV penetration levels (20%, 70% and 120%), and simulations were conducted using irradiance data from three different times of day (early morning, late morning, and midday). In this work, penetration level was defined as installed PV power divided by peak load. Assuming a 6 MW peak load, these PV penetration levels correspond to 1.2 MW, 4.2 MW and 7.2 MW installed capacity respectively. Both MATLAB and PSLF models were validated against PV power and frequency data collected at the 1.2 MW La Ola PV plant in Lanai for the 20% case.

A. Irradiance Data and the Wavelet Variability Model

Available PV power output was computed based on irradiance measured using a single LI-COR® silicon pyranometer at the 1.2 MW La Ola PV plant on Lanai [10]. Irradiance data was available at 1-second resolution. This irradiance point sensor was scaled to plant-average irradiance which accounts for the spatial smoothing across the array area for the PV plant. This allowed for simulation of any size PV plant; using measured power output from the La Ola plant would only be representative of the 1.2 MW case. In particular, the Wavelet Variability Model (WVM) [6] was used to smooth the irradiance at each simulation PV array location. The WVM applied different smoothing based on the amount of PV, the PV density, and the daily cloud speed (see Fig. 3). The PV density was assumed to be 40 W/m^2 for utility-scale PV plants (such as La Ola) and 5 W/ m^2 for distributed PV (i.e., rooftop). The daily cloud speed was assumed to be 10 m/s for Hawaii based on [11].

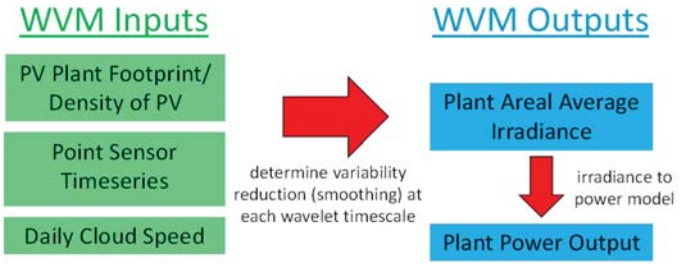

Fig. 3. Inputs and outputs for the wavelet variability model (WVM)

The output of the WVM was plant area average irradiance, which was converted into an available AC power value using the Sandia Array Performance Model (irradiance to DC) [12] and the Sandia Inverter Model (DC to AC) [13]. This procedure has been validated at other PV plants [8]-[9] and is expected to have similar accuracy at the Lanai location.

B. Irradiance Profiles

Irradiance profiles from four days were used for this study to cover a wide range of irradiance conditions and capture the system dynamics during the worst-case ramp rates:

- December 7th, 2010 – Least Variable
- September 3rd, 2010 – Average Variability
- April 23rd, 2011 – Largest Single Ramps
- November 4th, 2010 – Most Variable Total Day

Irradiance profiles for these four days are displayed in Fig. 4.

C. MATLAB Dynamic Model

To evaluate the effect of the frequency-watt function on power system performance over a full solar day (sunrise to sunset), a simplified model was developed in MATLAB. At the Miko power plant on Lanai. 2015 operations typically include two 2.8 MW diesel generators in a master-slave configuration providing isochronous control with additional 1.2 MW droop control diesel generators connected as needed to meet the island load.

In this model, the generators were aggregated and represented as one spinning mass, the governor controls were aggregated, and the PV power was summed. Fig. 5 shows the integrated Miko power plant model.

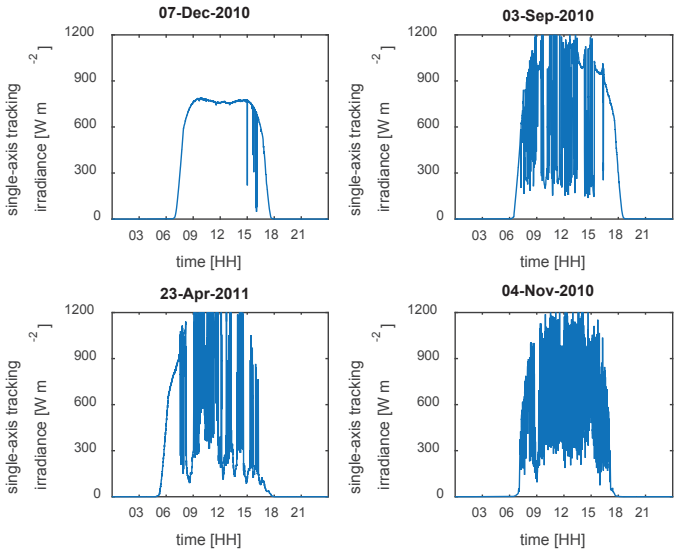

Fig. 4. Shows Irradiance profiles collected from the La Ola PV power plant showing (top left) little variability on Dec. 7th, 2010; (top right) typical variability seen on Sept. 3rd, 2010; (bottom left) April 23, 2011, largest single ramps; and (bottom right) day with highest total variability, Nov. 4th, 2010

With isochronous control, combustion time constant and rotor velocity, the system model is third order. The system dynamics were computed using four-step integration with fixed time step of 2 ms. Since the available PV power was computed using the WVM with 1-second resolution, intermediate values were determined at the smaller time step using linear interpolation. The available PV power and system frequency were then used to compute the PV power applied to the system using the frequency-watt function definition.

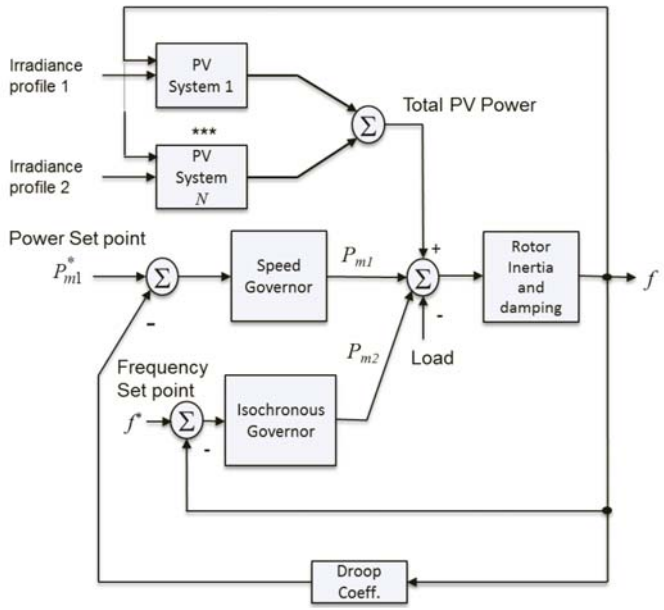

Fig. 5. Overview of the simplified power plant model which includes a mixture of droop and isochronous speed control as well as PV power from multiple locations

D. PSLF Model

GE's PSLF platform was used to evaluate the grid response to two grid event scenarios: generator outage and line-to-ground fault on a distribution line feeding a well pump. The PSLF model of the Lanai electricity grid includes the transmission system, substation transformers, diesel generators, and PV generators, such that high-fidelity transient system dynamics could be studied on short time scales (i.e. several minutes). To account for the time-varying PV power availability, PV power values were pre-computed using WVM and read into the 240 second PSLF simulations. Unlike the MATLAB model—wherein PV power was summed—in the PSLF model, individual PV plants and aggregated rooftop solar was simulated with inverter controller dynamics and connected to the appropriate bus in the circuit. The PSLF model included 49 buses for the 20% penetration case, 56 buses for the 70% penetration case and 59 buses for the 120% case. The model was based on previous work at Sandia National Laboratories [14].

Three pre-calculated irradiance profiles were created for the PSLF simulations to represent early morning (irradiance varies from 176 to 493 W/m^2), late-morning (irradiance varies from 292 to 1,033 W/m^2), and midday (irradiance varies from 1,012 to 1,147 W/m^2). The available PV power profiles were computed using WVM variability, which considers the density of installed PV panels, cloud speed and whether the panels are fixed or tracking. In the case of multiple PV plants, irradiance data was time-shifted based on geographical distance and 10 m/s cloud speed. For the 120% penetration case, three locations were considered: La Ola power plant with concentrated PV collection with single axis trackers, Lanai city with distributed PV collection using fixed plane rooftop solar, and the Manele Hotel with concentrated PV collection with single axis trackers. The available normalized PV power was computed for the nine cases (three locations and three times of day) and shown in Fig. 6.

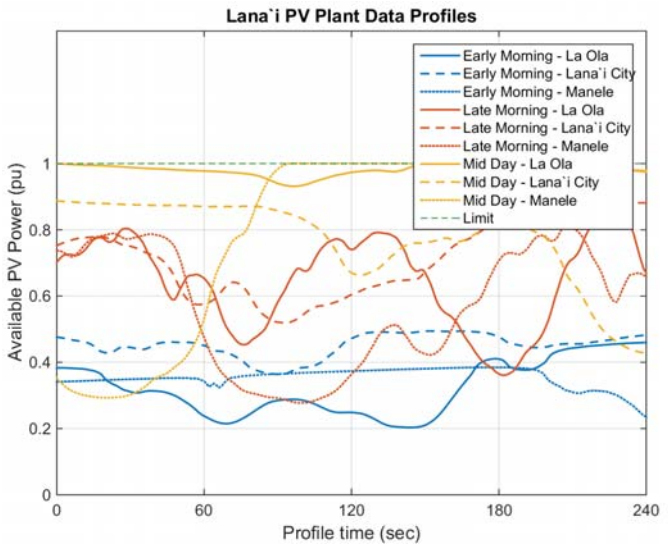

Fig. 6. Available PV power profiles computed for PSLF simulation for 120% PV penetration case; power values given in per unit (pu)

Finally, it is noted that the frequency-watt control would not be instantaneous. In practice, changes in inverter output power would lag behind measured frequency changes. Herein,

the PSLF inverter models were assumed to have a first-order response with 100 msec time constant for both increasing and decreasing output power.

E. Model Validation

The MATLAB and PSLF grid frequency simulations were validated using Lanai frequency data collected at the La Ola PV power plant for the 20% penetration case. The OSIsoft PI server data [15] contains time-synchronized PV power and frequency data. A six minute period of high PV variability was replayed in both the simplified MATLAB model and the PSLF system model to generate grid frequency data. A comparison of the grid frequency from the PI data and the two models is shown in Fig. 7.

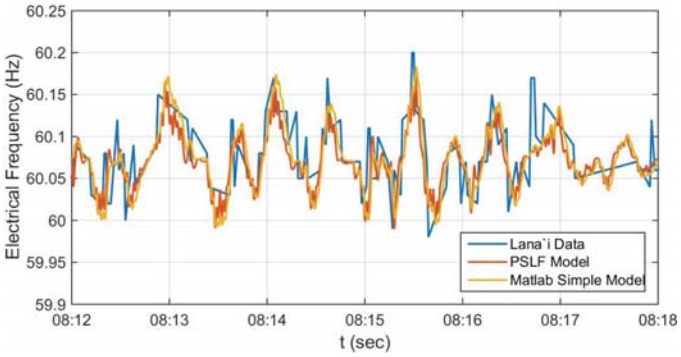

Fig. 7. Comparison of the Lanai frequency data to the MATLAB and PSLF simulations.

On inspection, there is good correlation between the MATLAB and PSLF model outputs and the measured frequency data. The simulation data was down sampled to correspond to the measured data, and the agreement was evaluated using the Pearson's correlation coefficient, computed over the six minute window, where $-1<\rho<1$ with $\rho=1$ being the best match. The Pearson's correlation coefficient relating the PSLF simulation result to La Ola data was $\rho=0.724$, relating the MATLAB result to La Ola data was $\rho=0.782$, and relating the two models was $\rho=0.939$. Thus, the models agree well with one another and moderately well with the data. It is noted that the load was constant in both models but was likely varying in the physical system, which would contribute to frequency variation.

III. Simulation Results

The effect of FW function parameters was evaluated in simulation using both the MATLAB and PSLF models. The MATLAB simulation example is presented first.

A. MATLAB Simulations

To illustrate performance of the PV system under high solar variability conditions and high penetration, the system is evaluated using the irradiance data from 4 Nov, 2010 with 70% PV penetration, and the system response was simulated using the FW curves defined in Fig. 8. Fig. 9 shows the output power, ramp rates, and frequency plotted over time. The ramp rate and grid frequency range performance metrics compared to lost PV power generation were obtained, as seen in Fig. 10.

The energy lost is defined as the percent difference between the PV energy output from a given curtailment scenario and the PV energy available with no curtailment. This percentage would represent the cost of implementing the frequency-watt function, depending on the price of electricity. However, as PV penetrations increase, PV systems may be curtailed anyway, so there would no longer be an economic penalty to enacting this control scheme.

The ramp rates were defined using the difference between samples of the output power, spaced 1-second apart. The frequency performance was determined by the difference between the maximum and minimum frequency experienced during the simulation of a day. It is noted in Figure 10b that a 15% capacity curtailment results in the 99% ramp rate dropping from 79.6 kW/sec to 78.6 kW/sec and the frequency range drops from 1208 mHz to just 1039 mHz: almost negligible benefit. However, with FW22 set 2, the 99% ramp rates drop to 50.0 kW/sec and frequency range is 739 mHz for a 2% loss of PV energy.

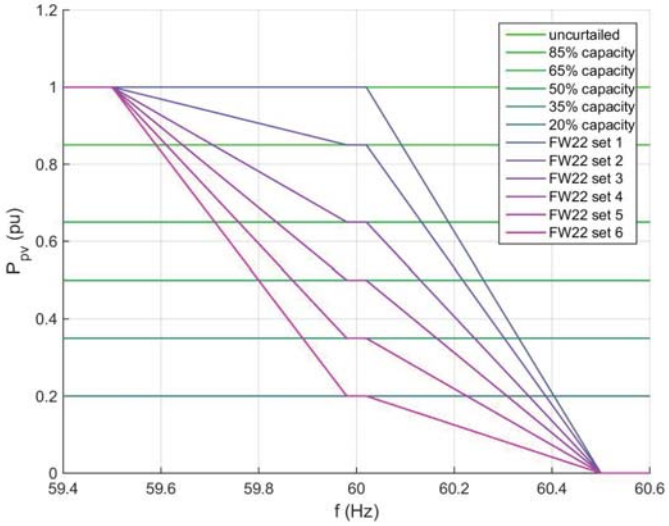

Fig. 8. Family of curves showing capacity curtailment and FW function defintions used in MATLAB study

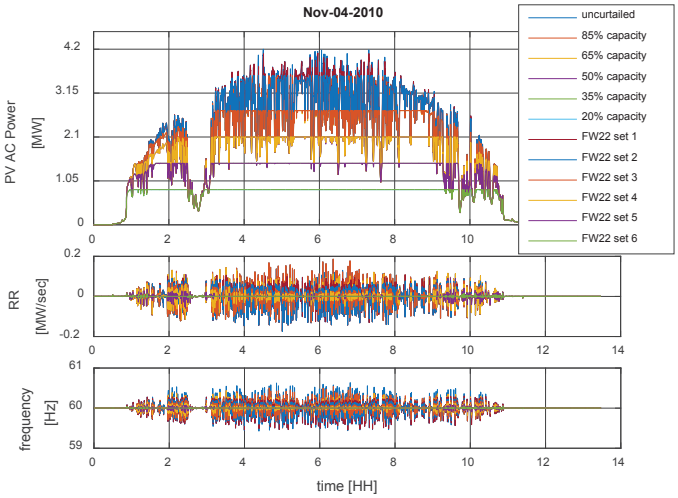

Fig. 9. Time domain plot of MATLAB simulation for 70% penetration case showing PV AC Power, Ramp Rates (RRs) and system frequency for variety of curtailment values and FW function definitions

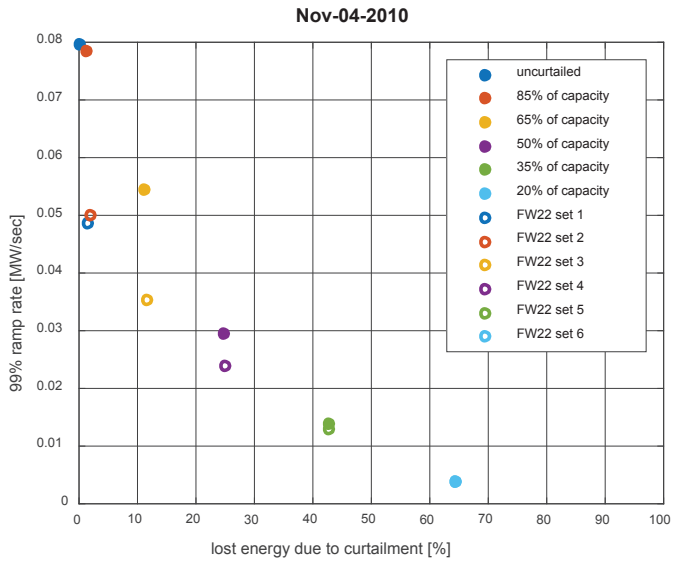

(a)

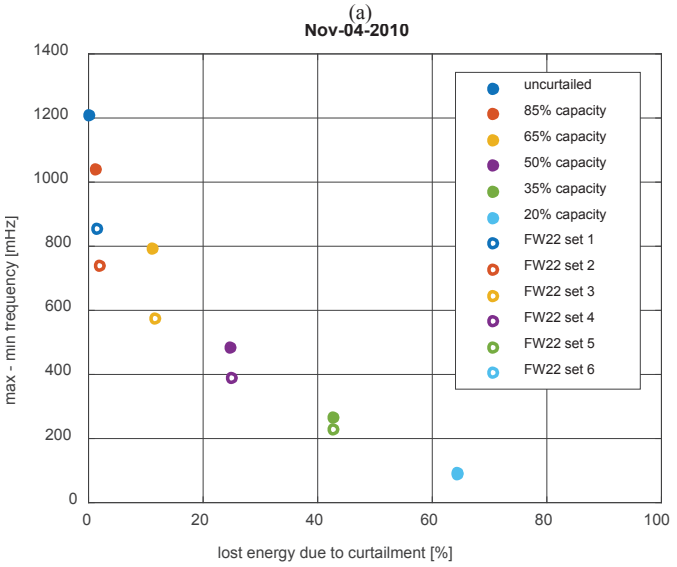

(b)

Fig. 10. Plot of (a) ramp rates vs energy loss and (b) frequency range vs energy loss for November 4th, 2010 dataset assuming 70% penetration

Similar benefits are seen for the April 23rd, 2011 dataset. Frequency range results are shown in Fig. 11, assuming again a 70% PV penetration. Therein, the base case results in 1566 mHz of range. When a simple 15% curtailment is applied, this range drops to 1415 mHz and results in 3.2% less energy. With a 35% curtailment, the range drops to 1166 mHz but costs 13.4% of the PV energy. The trade-off improves by applying the FW control. FW set 1 results in 1011 mHz range with 1% loss of energy, set 2 results in 902 mHz with 3.7% loss of energy, and set 3 results in 776 mHz with 13.6% loss.

The September 3rd, 2010 dataset is evaluated in Fig. 12 assuming 120% penetration (7.2 MW installed PV). In this case, a minimum curtailment is necessary since the installed capacity is greater than load. Therein, large benefits are demonstrated for the use of the FW function. For 35% curtailment, the system frequency deviates 1976 mHz and results in 13% energy loss, but the FW set 3 limits the frequency range to 1271 mHz with just 14.2% energy loss.

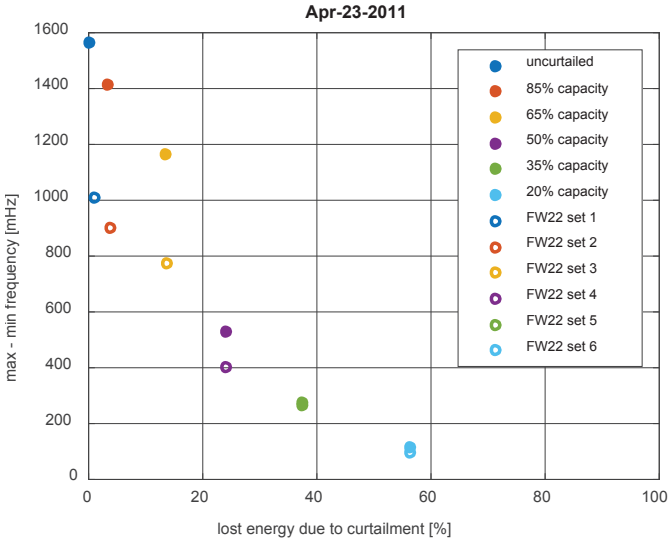

Fig. 11. Plot of frequency range vs energy loss for April 23rd, 2011 dataset assuming 70% penetration

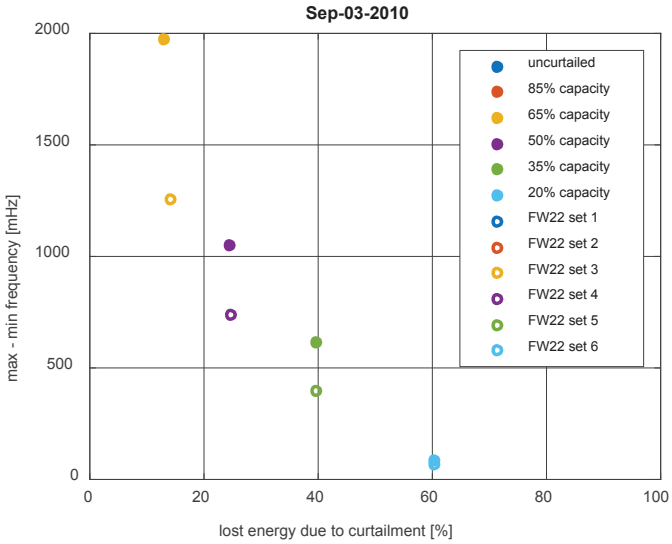

Fig. 12. Plot of frequency range vs energy loss for September 3rd, 2010 dataset assuming 120% penetration

As a final example, the December 7th, 2010 case assuming 20% PV penetration is shown in Fig. 13. In this low penetration clear-sky case, the frequency range is very small, and neither curtailment nor FW function implementation provides a benefit that is worth the loss of energy.

B. PSLF Simulations

To illustrate the benefits of the FW implementation during a contingency event, two examples are shown below comparing the FW function to PV active power curtailment. Both scenarios consider a 70% PV penetration scenario with late morning irradiance profile. The FW curve was defined with $GP_2 = GP_3$=0.6, 59.95 to 60.05 Hz deadband, and a droop of 80% of nameplate power/Hz; the curtailment was defined at

0.6 for all frequencies. Fig. 14a shows the simulated electrical frequency at the Miko power plant following loss of a 1.2 MW droop-controlled generator at t = 120 sec, and Fig. 14b shows the total PV power.

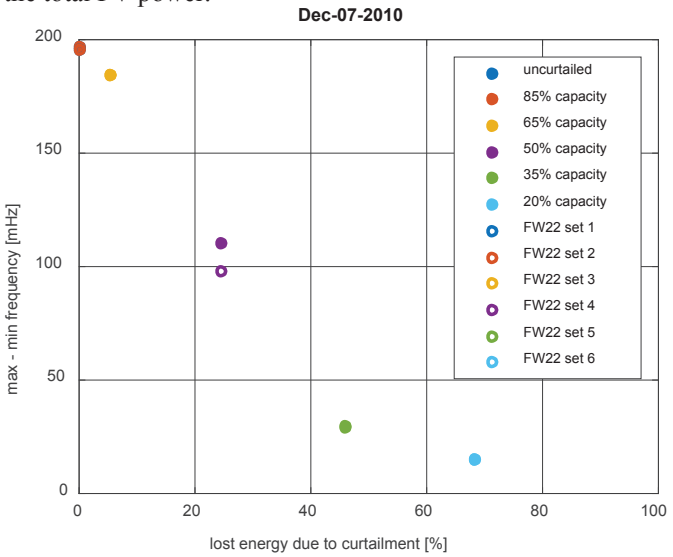

Fig. 13. Plot of frequency range vs energy loss for December 7th, 2010 dataset assuming 20% penetration

The FW and curtailment scenarios exhibit similar response to PV variation from t = 0-120 sec since they have the same limit at nominal frequency and frequency variation is primarily within the deadband of the FW function. However, following the loss of the 1.2 MW generator, a sizable drop in frequency is observed. Comparing the two responses, an improvement is seen in the frequency response with the FW implementation. The frequency drops to 59.32 Hz with simple curtailment, but the nadir is 59.52 Hz with the FW implementation. In addition, the generator speed rises to 60.11 Hz around t = 205 sec due to PV variation in the curtailment case, but is limited to 60.05 Hz in the FW implementation. The improvement is due to the FW control action. In particular, PV power rises by almost 223 kW (to full available power) in the FW case to compensate for the decrease in frequency following loss of generation; see Fig. 14b. The control action is best depicted, however, in the *power-frequency* phase plane together with the FW and curtailment limits; see Fig. 15. As the frequency falls below the deadband of the FW curve, the FW limit increases and PV power rises, helping the system to return to nominal frequency.

Fig. 16 shows results for the simulated line fault. The line-fault causes the generators to speed up. As with the previous example, the control action of the FW function mitigates the frequency deviation, resulting in a max frequency of f_{max_f} = 60.41 Hz compared to 60.70 Hz for the curtailment case. The resultant dynamic response results in a slightly lower minimum frequency of f_{min_f} = 59.80 Hz compared to 59.94 Hz for the curtailment case, however.

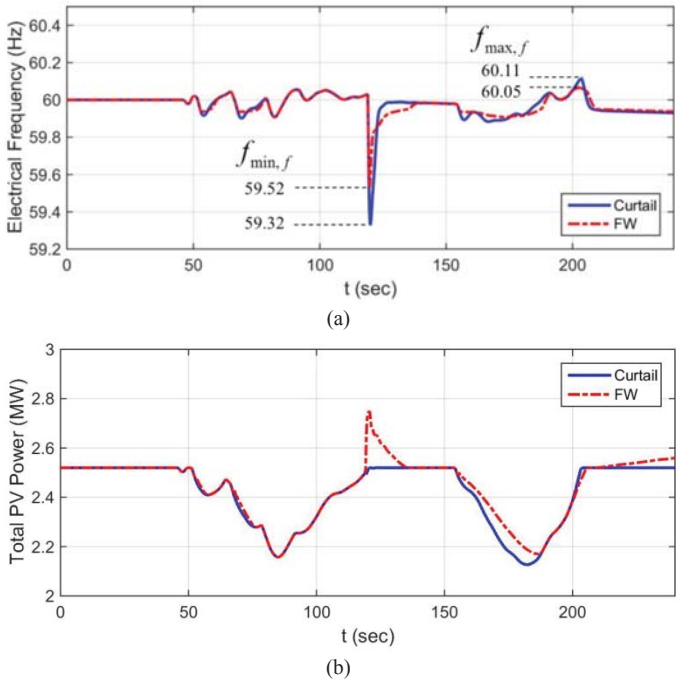

Fig. 14. Impact of FW and curtailment for simulated loss of 1.2 MW generator at t=120 sec showing (a) electrical frequency at the power plant and (b) total PV power

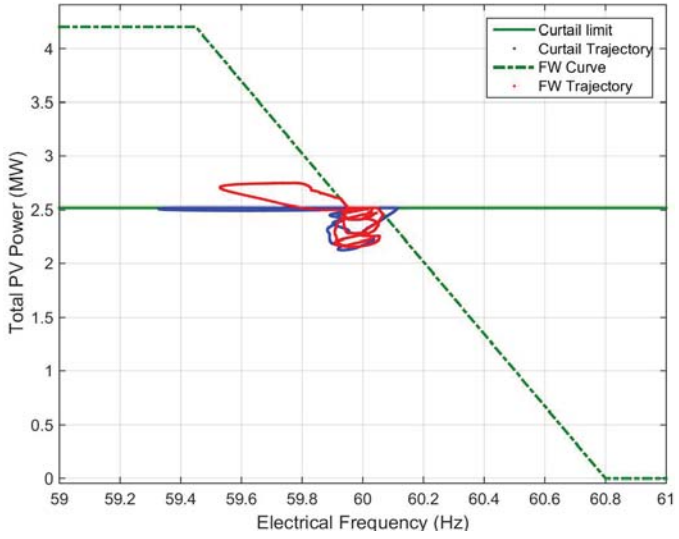

Fig. 15. FW implementation versus fixed curtailment, showing response in the PV power as generator speed varies

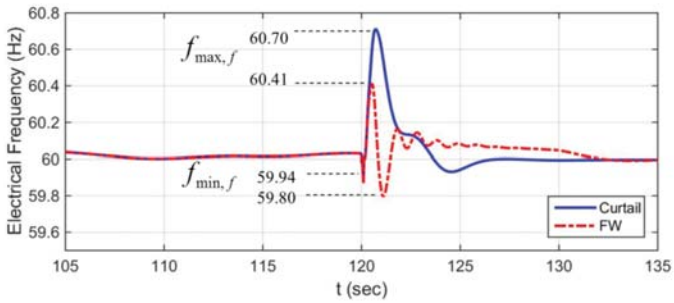

Fig. 16. Impact of FW and curtailment for simulated line fault at t=120 sec showing close-up of electrical frequency

IV. Experimental Results

To demonstrate the ability of frequency-watt implementation to mitigate frequency (generator speed) deviations, experiments were performed at DETL. These experiment configurations included a 225 kW diesel generator, a PV array simulator, a 24 kW inverter with frequency-watt functionality, a 50 kW resistive load, and a 25 kW resistive load. Four scenarios were considered: (a) the inverter operating with 100% of capacity with FW enabled, (b) the inverter operating with 100% of capacity with FW disabled, (c) the inverter operating at 50% of capacity with FW enabled, and (d) the inverter disconnected. Fig. 17 shows the configuration of the experimental setup, and Fig. 18 shows the FW function settings used in the inverter for scenarios (a) and (c). Therein, F_3 = 60.5 Hz and F_4 = 62.0 Hz.

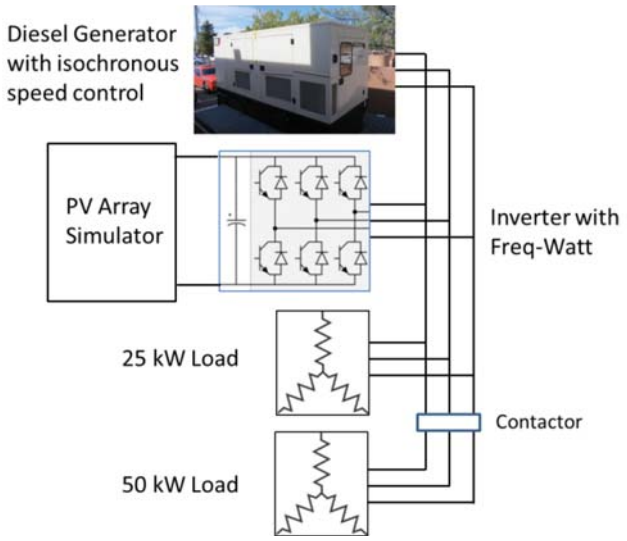

Fig. 17. Experimental test setup including diesel generator, PV inverter equiped with frequency-watt capability and loads.

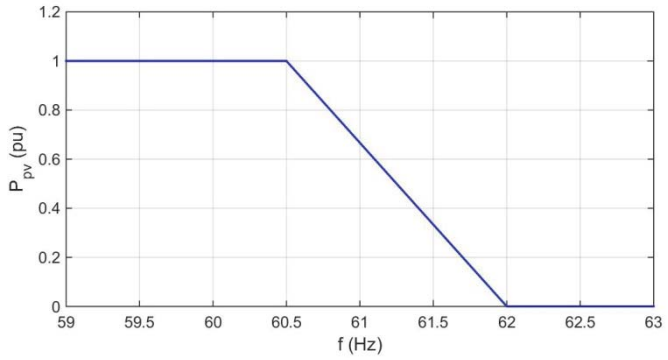

Fig. 18. FW function settings used for hardware experiments

Under all cases, the DC power available to the inverter was set to the DC input rating of the inverter using a PV array simulator. In case (c) the inverter is commanded to operate at 50% of rated active power. Fig. 19 shows the frequency response when the load is stepped from 75 kW to 25 kW by opening a contactor. In each case, generator speed increases rapidly after the load shed, but the peak frequency is lessened and then the return to nominal speed is improved in the cases with frequency-watt capability enabled. Only the case of increasing grid frequency was tested because of the limits in the inverter FW settings. Specifically, in this particular inverter, it was not possible to set up the FW parameters to allow power increase when f<F_2 because it was designed for the German grid code requirement VDE-AR-N 4105 [16].

To quantitatively compare the frequency performance of each scenario, a figure of merit was chosen to represent overall frequency deviation with time: $f_e = \int_{t_0}^{t_s}(f(\tau) - f^*)^2 d\tau$, where f_e is the integral square frequency error, expressed in Hz^2·s, or simply Hz; f is the system frequency; f^* is the scheduled frequency; t_0 is the time that the step change in the load occurs; and t_s is the time at which the frequency transient settles. The error is calculated over a 5-second time period. Another figure of merit is the total PV power generation before the event. Results are shown in Table 1. Therein, it is noted that the first case demonstrates the best frequency response and the greatest PV power penetration for this set of experiments. The same PV penetration occurs in the second case, but f_e is greater. The third case has a similar f_e as the first, but the PV penetration is half. The final case has slightly lower f_e than the second but includes no PV power.

Table 1: Performance comparison for a 75 kW to 25 kW stepped load

Scenario	Integral Squared Frequency Error f_e (Hz)	Initial PV Power (kW)
Inverter at 100% capacity with FW enabled	0.50993	24.0
Inverter at 100% capacity with FW disabled	0.75181	24.0
Inverter at 50% capacity with FW enabled	0.51738	12.0
Diesel generator with no inverter	0.61614	0.0

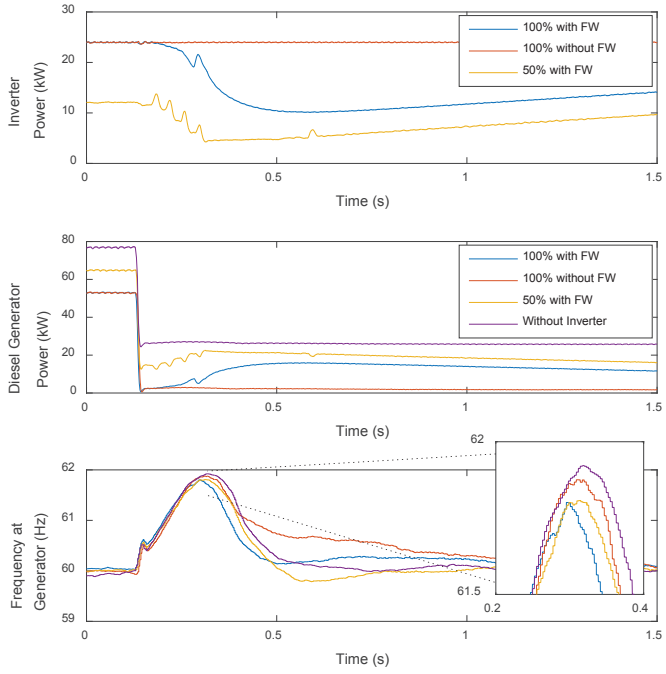

Fig. 19. Response to a 75 kW to 25 kW step change in load

This demonstration was intended to represent frequency variations that occur with 100-200 msec rise-times on a small electrical grid (much smaller than the Lanai power system). The frequency-watt control does exhibit a small lag in responding to a positive frequency (power reduction) swing, which is evident in Fig. 19, but the control is still effective for this experiment. However, it is noted that the power is slow to rise after the frequency returns to nominal. The exact cause of this is unknown but may be an intentional ramp limit. This slow response time could reduce the effectiveness of the control to compensate for drops in frequency.

Frequency events in the continental US would experience slower frequency changes than what is modeled and demonstrated here; thus, it is expected that FW control could provide effective frequency support in a larger grid. However, to be most effective, work is needed to ensure that the inverter response time is sufficiently small for both increasing and decreasing power output (in response to falling and rising frequency respectively), and that FW parameters can be adjusted to allow for power increase when $f<F_2$.

V. Conclusions and Future Work

In this work, use of the frequency-watt function to mitigate frequency deviations in a power system with high penetration of PV power is investigated. Using models of an island grid that have been validated against field-data, the approach is demonstrated in simulation, and the trade-off between renewable energy production and frequency deviation is quantified. The simulations show that using frequency-watt functionality and fixed curtailment both improve the frequency deviations on the grid during normal operation and during fault transients, but the frequency-watt functions provide a greater improvement for a given curtailment level. Furthermore, feasibility of implementing the frequency-watt function in an electrical system experiencing a loss of load fault was demonstrated using a hardware testbed.

In the future, the research team plans to investigate the optimal FW settings to provide frequency regulation and contingency reserve capabilities while minimizing the loss of PV power from curtailment. The team also plans to develop specifications and recommendations for limits on inverter response time.

References

[1] V. Gevorgian, S. Booth, Review of PREPA Technical Requirements for Interconnecting Wind and Solar Generation, NREL technical report, NREL/TP-5D00-57089, Nov. 2013.

[2] Hawai‘i Natural Energy Institute, Summary Review of Advanced Inverter Technologies for Residential PV Systems, Sept. 2014.

[3] J. Johnson, B. Schenkman, J. Quiroz, and A. Ellis, “Initial operating experience of the La Ola 1.2 MW photovoltaic system,” Sandia National Laboratories Technical Report SAND2011-8848, 2011.

[4] The Mathworks, Inc., MATLAB the language of technical computing, 3 Apple Hill Drive, Natick, MA 01760-2098 USA.

[5] IEC Technical Report 61850-90-7, “Communication networks and systems for power utility automation–Part 90-7: Object models for power converters in distributed energy resources (DER) systems,” Edition 1.0, Feb 2013.

[6] M. Lave, J. Kleissl, and J. S. Stein, "A Wavelet-Based Variability Model (WVM) for Solar PV Power Plants," Sustainable Energy, IEEE Transactions on, pp. 1-9, 2012.

[7] M. Lave and J. Kleissl, "Cloud speed impact on solar variability scaling – Application to the wavelet variability model," Solar Energy, vol. 91, pp. 11-21, 2013.

[8] M. Lave and J. Kleissl, "Testing a wavelet-based variability model (WVM) for solar PV power plants," in IEEE Power and Energy Society General Meeting, 2012.

[9] M. Lave, J. Kleissl, and J. S. Stein, "A Wavelet-Based Variability Model (WVM) for Solar PV Power Plants," IEEE Transactions on Sustainable Energy, 2013.

[10] S. Kuszmaul, A. Ellis, J.S. Stein, L. Johnson, Lanai High-Density Irradiance Sensor Network for characterizing solar resource variability of MW-scale PV system, 35th IEEE Photovoltaic Specialists Conference (PVSC), Honolulu, HI, 2010.

[11] L. M. Hinkelman, "Differences between along-wind and cross-wind solar irradiance variability on small spatial scales," Solar Energy, vol. 88, pp. 192-203, 2013.

[12] D. King, W. Boyson, and J. Kratochvil, "Photovoltaic Array Performance Model," SAND2004-3535, 2004.

[13] D. King, S. Gonzalez, G. Galbraith, and W. Boyson, "Performance Model for Grid-Connected Photovoltaic Inverters," SAND2007-5036, Sandia National Laboratories, 2007.

[14] KEMA, Inc., Lanai PV Interconnect Requirements Study: System Impact Study, June 5, 2008, Interconnection Customer: SunPower, KEMA, Inc., Raleigh, NC, USA, 26707.

[15] OSIsoft, The PI System - the industry standard in enterprise infrastructure for management of real-time data and events, visited 22 Nov, 2015, URL: https://www.osisoft.com/software-support/what-is-pi/What_Is_PI.aspx.

[16] VDE Reference “VDE-AR-N 4105 Power generation systems connected to the low voltage distribution network -Technical minimum requirements for the connection to and parallel operation with low voltage distribution networks”, Aug. 2008.